Acta Crystallographica Section D
Biological Crystallography
ISSN 0907-4449

Structural basis of L-phosphoserine binding to *Bacillus alcalophilus* phosphoserine aminotransferase

Pradeep Battula, Anatoly P. Dubnovitsky‡ and Anastassios C. Papageorgiou*

Turku Centre for Biotechnology, University of Turku and Åbo Akademi University, BioCity, FIN-20521 Turku, Finland

‡ Present address: Department of Clinical Neurosciences, Center for Molecular Medicine L8:04, Karolinska Institutet, SE-17 176 Stockholm, Sweden.

Correspondence e-mail: tassos.papageorgiou@btk.fi

Received 28 September 2012
Accepted 21 January 2013

PDB References: *Ba*PSAT–PSER complex, 4azj; free *Ba*PSAT, 4azk

Phosphoserine aminotransferase is a vitamin B_6-dependent enzyme that catalyzes the reversible conversion of 3-phosphohydroxypyruvate to L-phosphoserine using glutamate as an amine donor. In an effort to gain insight into the substrate-recognition mechanism of the enzyme, crystal structures of *Bacillus alcalophilus* phosphoserine aminotransferase in the presence or absence of L-phosphoserine were determined to resolutions of 1.5 and 1.6 Å, respectively. Local conformational changes induced upon substrate binding were identified. However, in contrast to other aminotransferases, no domain or subunit movements were observed. Two Arg residues (Arg42 and Arg328) and two His residues (His41 and His327) were found to form a tight binding site for the phosphate group of L-phosphoserine. Comparison with *Escherichia coli* phosphoserine aminotransferase in complex with the substrate analogue α-methylglutamate revealed more extensive structural changes in the case of L-phosphoserine binding. Based on the structural analysis, the flexibility of Arg328 is proposed to be critical for substrate recognition.

1. Introduction

Phosphoserine aminotransferase (PSAT; EC 2.6.1.52) catalyzes the reversible conversion of 3-phosphohydroxypyruvate to L-phosphoserine in a ping-pong bi-bi mechanism (Basurko *et al.*, 1999),

$$\text{3-phosphohydroxypyruvate} + \text{L-glutamate} \longleftrightarrow \text{L-phosphoserine} + \text{2-oxoglutarate}.$$

This reaction is the second step of the major pathway of L-serine biosynthesis in many organisms from bacterial cells to mammals, including humans. After its formation, L-phosphoserine is dephosphorylated by L-phosphoserine phosphatase (EC 3.1.3.3) to yield L-serine, which subsequently acts as the major source of single-carbon fragments and as a precursor of cysteine and phospholipid- and sphingolipid-glycine. L-Serine can be further utilized as a precursor of glycine *via* a serine hydroxymethyltransferase-catalyzed reaction. Several disorders associated with serine biosynthesis have been reported (de Koning *et al.*, 2003).

Two isoforms of PSAT produced through alternative splicing have been reported in humans (Baek *et al.*, 2003). Recent studies have identified the human PSAT1 isoform as a pro-proliferative and pro-survival factor in colon cancer (Vié *et al.*, 2008). PSAT1 mRNA levels have been found to be elevated in colon adenocarcinoma and to increase with tumour stage in colon cancer (Ojala *et al.*, 2002). Furthermore, high PSAT1

Table 1
Data-collection and refinement statistics.

Values in parentheses are for the outermost resolution shell.

	*Ba*PSAT–PSER complex	Free *Ba*PSAT
Data collection		
Wavelength (Å)	1.097	0.811
Space group	$C222_1$	$C222_1$
Unit-cell parameters (Å)	a = 104.7, b = 136.2, c = 151.3	a = 105.6, b = 136.6, c = 152.0
No. of molecules per asymmetric unit	2	2
Resolution range (Å)	20.0–1.5 (1.54–1.50)	40.0–1.6 (1.65–1.60)
No. of measured reflections	692954	458775
Unique reflections	170566	144217
Completeness (%)	99.4 (99.5)	99.2 (95.5)
Mosaicity (°)	0.367	0.767
$\langle I/\sigma(I)\rangle$	12.9 (2.2)	10.9 (1.6)
$R_{\rm merge}$	0.063 (0.329)	0.034 (0.234)
Wilson B factor (Å^2)	15.7	17.0
Refinement		
Reflections (working/test)	161909/8635	136850/7292
$R_{\rm cryst}/R_{\rm free}$	0.146/0.165	0.153/0.170
No. of protein atoms	5827	5730
No. of water molecules	1126	1106
No. of PLP–PSER atoms	52	—
Stereochemistry		
R.m.s.d. bond lengths (Å)	0.012	0.012
R.m.s.d. bond angles (°)	1.47	1.46
Ramachandran favoured (%)	98.0	98.0
Ramachandran outliers (%)	0	0
Clashscore	7.2	7.2
Coordinate error†	0.07	0.08
Average B factors (Å^2)		
Protein	15.4	16.6
Water	31.5	30.6
PLP–PSER	11.0	—

† Based on diffraction-component precision index calculations (Cruickshank, 1999).

mRNA levels in breast cancer have been associated with a poor clinical response to endocrine therapy. Accordingly, human PSAT1 has been suggested as a potential drug target in cancer therapy (Pollari *et al.*, 2011).

PSAT acts as a homodimer and contains one pyridoxal 5′-phosphate (PLP) molecule per monomer as a cofactor attached to the ε-amino group of a Lys residue through a Schiff base. The two active sites are found at the subunit–subunit interface. In all PLP-dependent enzymes, including PSAT, the covalently bound PLP forms an internal aldimine. With the exception of glycogen phosphorylase, the internal aldimine is replaced by an external aldimine between PLP and the substrate amino group at the beginning of the catalytic cycle.

PSAT and other aminotransferases (ATs) use a dual substrate-recognition mechanism that enables them to recognize two different amino acids (Hirotsu *et al.*, 2005). Accordingly, a complete understanding of the catalytic mechanism in ATs requires structural knowledge of the binding details of each substrate. The crystal structure of *Escherichia coli* PSAT (*Ec*PSAT) with a substrate analogue (α-methylglutamate; AMG) has previously been elucidated at medium resolution (Hester *et al.*, 1999). Here, we present the crystal structures of *Bacillus alcalophilus* PSAT (*Ba*PSAT) at high resolution with and without L-phosphoserine (PSER) bound. In contrast to the *Ec*PSAT–AMG complex, the binding of PSER induces significant local changes at the active site of *Ba*PSAT–PSER. Moreover, the PLP ring in *Ba*PSAT was found to be only slightly rotated, in contrast to the larger rotation observed in the *Ec*PSAT–AMG complex. No changes at the domain or subunit level were observed upon substrate binding in both *Ba*PSAT and *Ec*PSAT. These observations could be useful in better understanding the mechanistic details of the catalytic reaction in PSAT and may form a basis for the design of selective human PSAT inhibitors as potential drugs.

2. Materials and methods

2.1. Expression, purification and crystallization

Recombinant *Ba*PSAT was expressed in *E. coli* cells, purified and crystallized as described previously (Dubnovitsky *et al.*, 2003). Crystals were grown by the hanging-drop vapour-diffusion method in Linbro 24-well cell-culture plates. The drops consisted of 2 µl protein solution (10–15 mg ml^{-1} in 10 m*M* Tris–HCl pH 8.0) and 2 µl reservoir solution (1.4 *M* trisodium citrate dihydrate, 0.1 *M* Tris–HCl pH 8.5). The drops were equilibrated against 700 µl reservoir solution at 289 K. Crystals appeared after 1 d. The *Ba*PSAT–PSER complex was obtained by cocrystallization of the enzyme with 25 m*M* L-phosphoserine. The crystallization conditions were the same as those used for free *Ba*PSAT.

2.2. Data collection

All data were processed, scaled and integrated with *HKL*-2000 (Otwinowski & Minor, 1997). Data for the *Ba*PSAT–PSER complex were collected on beamline I711 at MAX-lab (Lund, Sweden) at a wavelength of 1.097 Å. A single crystal was used after it had briefly been soaked in reservoir solution containing 15%(*v*/*v*) glycerol as a cryoprotectant. The crystal was subsequently placed in a stream of gaseous N_2 at 100 K. A high-resolution pass (1.5 Å, 160 images, 0.5° rotation) was initially employed followed by a low-resolution pass (2.0 Å, 133 images, 0.5° rotation), resulting in a complete data set to 1.5 Å resolution.

Diffraction data for the free *Ba*PSAT structure were collected to 1.6 Å resolution on beamline X13 at EMBL, Hamburg (λ = 0.811 Å). 196 images were collected with 0.4° rotation. Detailed data-collection statistics are presented in Table 1.

2.3. Structure determination and refinement

Initial phases were obtained by molecular replacement using *Phaser* (McCoy *et al.*, 2007) with the coordinates of *Ba*PSAT in space group $P2_12_12$ determined previously at a resolution of 1.08 Å (Dubnovitsky, Kapetaniou *et al.*, 2005) as the search model. The structure was refined with *PHENIX* (Adams *et al.*, 2010). Restraints for PLP–PSER were created with *eLBOW* (Moriarty *et al.*, 2009). The same set of reflections was used in the R_{free} calculations for both free and PSER-bound *Ba*PSAT.

Visualization of the structures and manual rebuilding were performed with *Coot* (Emsley & Cowtan, 2004). Analysis of the final structures was carried out with *MolProbity* (Chen *et al.*, 2010), *POLYGON* (Urzhumtseva *et al.*, 2009) and various diagnostic tools implemented in *Coot* and *PHENIX*. Detailed refinement statistics are presented in Table 1. Structural superpositions were performed with *PDBeFold* (Krissinel & Henrick, 2004) and were subsequently used for structure-based sequence alignment.

3. Results

3.1. Quality of the structures

*Ba*PSAT and *Ba*PSAT–PSER crystallize as dimers in the asymmetric unit. The structure of *Ba*PSAT–PSER was determined at 1.5 Å resolution and refined to a final R_{cryst} and R_{free} of 0.146 and 0.165, respectively. There are 5827 protein atoms, 1126 water molecules, two chloride ions and two molecules of PLP in the asymmetric unit. Each PLP molecule is linked through a Schiff base to PSER at the C4′ atom of the cofactor. 36 residues were modelled with alternative conformations. The unligated *Ba*PSAT structure was determined at a resolution of 1.6 Å and refined to an R_{cryst} of 0.153 (R_{free} = 0.170). The final structure is of good quality and is comparable to the *Ba*PSAT–PSER complex structure. 20 residues were identified with double conformations. PLP was found to be connected to Lys196, as shown by continuous electron density. There are two surface loops, both in subunit *A*, that are characterized by high flexibility: 211–218 and 326–331. Inspection of the two subunits shows that these loops are more ordered and better defined in subunit *B*; thus, subunit *B* will be used for most of the comparisons. The loop 211–218 in subunit *A* is close to a symmetry-related molecule in the crystal lattice. Although it appears to adopt a double conformation, the additional electron density did not permit the building of the second conformation. Thus, residues 213–217 of subunit *A* were assigned half occupancy during refinement, but the refined occupancies did not improve the quality of the map.

3.2. Overall structure

The two subunits of *Ba*PSAT–PSER are related by twofold noncrystallographic symmetry (Fig. 1). The r.m.s.d. between the two subunits is 0.27 Å, suggesting that there are no significant differences between them. Comparison with the previously determined *Ba*PSAT structure in space group $P2_12_12$ revealed the highest similarity (r.m.s.d. of 0.31 Å) to be between subunit *B* of *Ba*PSAT–PSER and subunit *A* of the least radiation-damaged *Ba*PSAT structure (structure *A*; PDB entry 2bhx; Dubnovitsky, Ravelli *et al.*, 2005). The main differences are found in the loops involved in PSER binding, as will be explained later. In addition, a loop (213–217) missing from the $P2_12_12$ *Ba*PSAT structure has been modelled in the new structure. Overall, the structure of each subunit consists of two domains: a small domain (residues 267–360 together with the N-terminal residues 1–15) and a large domain (residues 16–266). The latter contains a mixed seven-stranded sheet (β2–β5 and β8–β10). The loop connecting strand β9 (residues 189–193) to strand β10 (residues 204–209) harbours the active-site residue Lys196.

3.3. Structural comparisons

Comparison with the unligated *Ba*PSAT structure gives the best superposition when the *B* subunits are structurally aligned, resulting in an r.m.s.d. of 0.36 Å in C^{α}-atom positions (Fig. 1). The main deviations are found at residues 325–333 and 40–46. In particular, *B*:Arg328 and *A*:Arg42 show a significant change (>3.0 and 0.8 Å, respectively) in main-chain position that brings them closer to the active site (Fig. 2). However, the side chain of *B*:Arg328 undergoes a larger movement (∼7 Å) and a rotation of approximately 60° that contributes to the formation of a binding site for the phos-

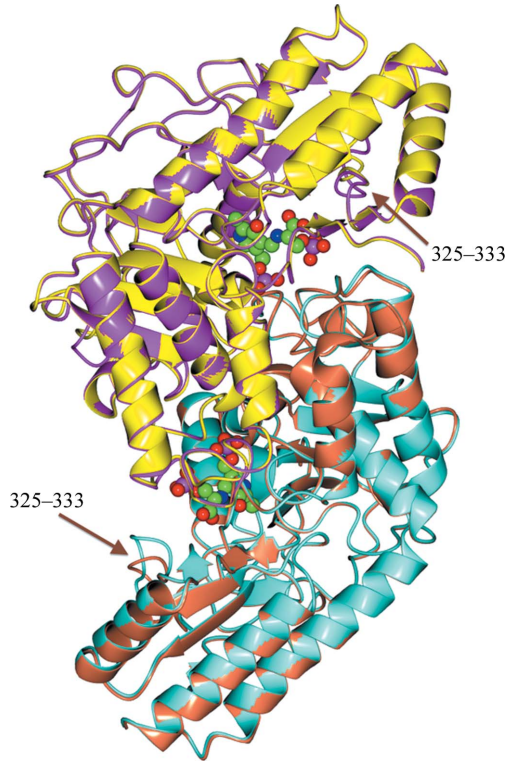

Figure 1
Superposition of the *Ba*PSAT–PSER structure (the *A* and *B* subunits are coloured magenta and cyan, respectively) onto the free *Ba*PSAT structure (the *A* and *B* subunits are coloured yellow and coral, respectively). PLP and bound PSER are shown in sphere representation. The position of loop 325–333 is indicated by arrows. The secondary-structure elements were assigned based on *DSSP* (Kabsch & Sander, 1983). The figure was drawn using *CCP4mg* (McNicholas *et al.*, 2011).

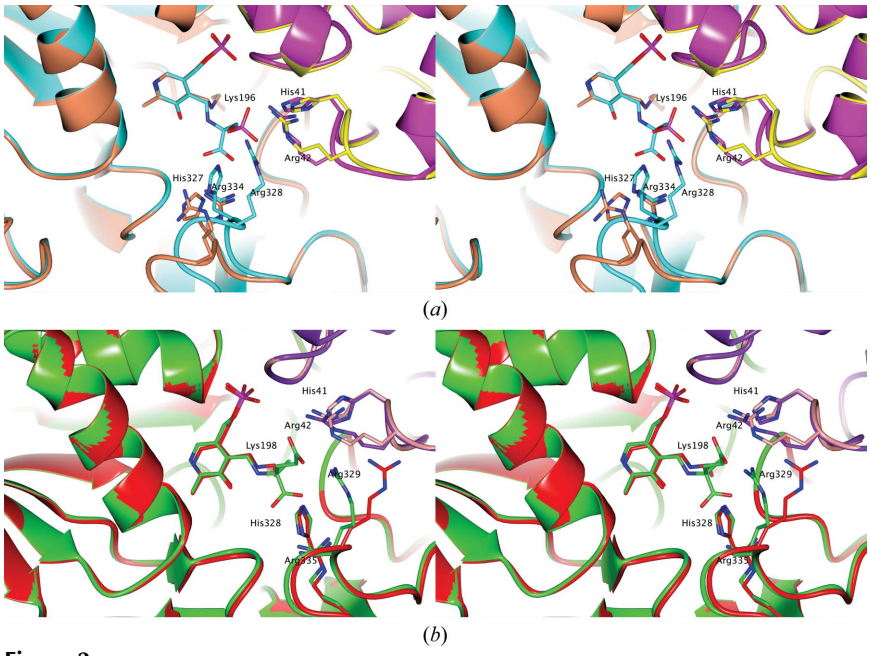

Figure 2
Close-up stereoview of the conformational changes at the active site of (*a*) *Ba*PSAT and (*b*) *Ec*PSAT. The colour scheme for *Ba*PSAT–PSER and *Ba*PSAT is the same as in Fig. 1. The free *Ec*PSAT *A* and *B* subunits are shown in red and pink, respectively, and those of *Ec*PSAT–AMG are shown in green and purple, respectively. PLP, PLP–PSER, PLP–AMG and side chains are shown in stick representation. The active-site residues Lys196 (*Ba*PSAT) and Lys198 (*Ec*PSAT) are also depicted.

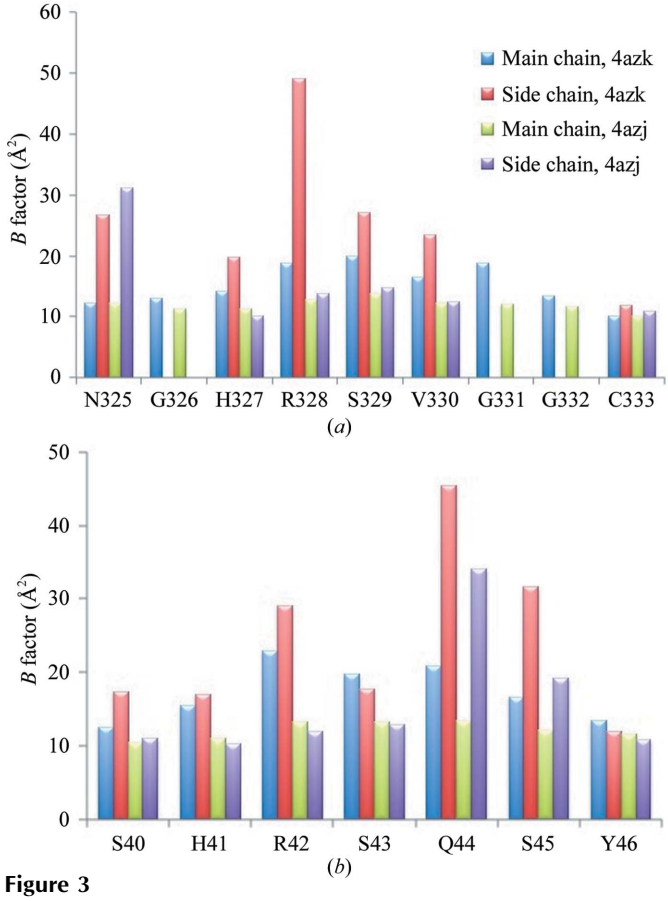

Figure 3
Schematic diagram of the temperature-factor changes upon substrate binding in *Ba*PSAT: (*a*) loop 325–333, (*b*) loop 40–46.

phate group of PSER. As a result of this conformational change, *B*:Arg328, which is solvent-exposed in the free structure, becomes buried in the complex. Both *B*:Arg328 and *A*:Arg42 are flexible in the free *Ba*PSAT structure, with average temperature factors of 40 and 38 Å^2 for the guanidium groups, respectively. Upon formation of the complex, these two residues are stabilized and their temperature factors are reduced to around 14 Å^2. A significant drop in the temperature factors (∼10 Å^2 for the side chains) is also observed for the respective loops 325–333 and 40–46 (Fig. 3).

Structural comparison with the 1.68 Å resolution structure of free *Ba*PSAT in space group $P2_12_12$ was also carried out and confirmed the conformational changes in *Ba*PSAT–PSER for the main-chain and side-chain atoms of loops 325–333 and 40–46, although to a different extent. Thus, for instance, the main-chain atoms of Arg328 and Arg42 move 1.6 and 1.2 Å closer to the active site, respectively, upon PSER binding (Supplementary Fig. S1[1]). Importantly, the average temperature factors for the loops 325–333 and 40–46 (29.0 and 23.3 Å^2, respectively) are higher than the average temperature factors for the whole protein (20.0 Å^2). The side chains of Arg328 and Arg42, in particular, have average temperature factors of 93.0 and 38.4 Å^2, indicating flexibility in the absence of substrate.

Additional conformational changes upon PSER binding are observed in *B*:His327 and *A*:His41. *B*:His327 moves approximately 2 Å closer to the active site, although in subunit *A* the move is less significant (1.4 Å). In its new position, *B*:His327 NE2 is hydrogen-bonded (2.8 Å) to O6P, whilst its ND1 atom is hydrogen-bonded to Ser329 OG (distance of 2.8 Å), an interaction that probably further stabilizes the new position of His327. Notably, Ser329 adopts a different rotamer in the complex structure ($\chi_1 = 64.0^\circ$) compared with that in the free structure ($\chi_1 = -65.0^\circ$). *A*:His41 NE2 is at a hydrogen-bonding distance from O5P (2.9 Å) and interacts weakly with O7P (3.5 Å). Furthermore, upon binding of PSER seven water molecules are replaced and are not present in the complex.

The cofactor PLP is found in the form of an external aldimine in the *Ba*PSAT–PSER complex. Lys196 NZ forms a van der Waals contact with C4′ (3.1 Å). PLP is stabilized in its position by hydrogen bonds to Thr152 OG1 and Asp172 OD2 through the O3′ (2.5 Å) and N1 (2.7 Å) atoms (Fig. 4). In the free *Ba*PSAT the interactions are essentially similar. A prominent stacking interaction with Trp102 characterized by an almost perfect parallel alignment of the aromatic rings is

[1] Supplementary material has been deposited in the IUCr electronic archive (Reference: TZ5018). Services for accessing this material are described at the back of the journal.

present and contributes to the stabilization of PLP in both structures. The separation between the two rings is approximately 3.5 Å.

The subunit–subunit interface of *Ba*PSAT–PSER encompasses 2340 Å^2 of solvent-accessible area and involves 63 residues that give rise to 28 hydrogen bonds. The interface is mostly formed by residues from the large domain. In the free *Ba*PSAT structure there is a slight reduction in the solvent-accessible area (2190 Å^2) and in the number of hydrogen bonds (26), suggesting only subtle differences at the interface upon formation of the complex.

3.4. Comparison with the *Ec*PSAT–AMG complex

Structural comparison of the *Ba*PSAT–PSER complex with that of *Ec*PSAT–AMG (PDB entry 1bjo; Hester *et al.*, 1999) was carried out to compare the binding modes of the two different substrates in the catalytic reaction. The two O atoms, OXT and O, of the α-carboxylate group in PSER form a salt bridge and hydrogen bond to Arg334, a conserved residue that corresponds to Arg335 in *Ec*PSAT (Fig. 5). No significant changes are observed for Arg334, apart from a slight movement (approximately 0.13 Å). In the *Ec*PSAT–AMG complex the α-carboxylate group of AMG is far away from Arg335 (3.95 Å for O and 3.6 Å for OXT) and thus is unable to make strong interactions with Arg335. Ser9 of *Ec*PSAT has also been implicated in interactions with the α-carboxylate group of AMG. This residue corresponds to an Ala residue in *Ba*PSAT, *Bacillus circulans* var. *alkalophilus* PSAT (PDB entry 1w3u; Kapetaniou *et al.*, 2006) and *Yersinia pestis* CO92 PSAT (PDB entry 3qbo; Center for Structural Genomics of Infectious Diseases, unpublished work), while human PSAT (PDB entry 3e77; Structural Genomics Consortium, unpublished work) exhibits a three-residue deletion in the same region.

A slight rotation of PLP (by about 5°) in *Ba*PSAT–PSER appears to take place with no other significant changes in the PLP position (Fig. 6). In *Ec*PSAT–AMG the PLP ring is rotated by about 20° when the external aldimine is formed.

In *Ec*PSAT–AMG only subunit *A* has bound AMG. The active site in subunit *B* of *Ec*PSAT–AMG is inaccessible to the solvent owing to lattice contacts and is therefore unable to bind AMG. The temperature factors for AMG are in the range 70–80 Å^2, while calculation of the electron-density map using the Electron Density Server (http://eds.bmc.uu.se/eds/) shows weak density for AMG in subunit *A*. These features are most likely to indicate low occupancy of AMG in the *Ec*PSAT–AMG complex.

Furthermore, in the *Ec*PSAT–AMG complex Arg42 and Arg77 interact with the γ-carboxylate group of AMG. Arg77, in particular, has been suggested to play a dual role in both PLP binding and substrate binding. In *Ba*PSAT Arg77 is replaced by Ser77, which makes a hydrogen bond to O3P of PLP in both the complex and the free form but makes no contacts with the substrate. Instead, Lys105 from the neighbouring subunit appears to play the role of Arg77 in substrate binding as it is situated close to the phosphate group of the substrate and could maintain the positive electrostatic charge around the substrate.

A:Arg77 has been modelled in a double conformation in the free *Ec*PSAT structure, but in the AMG complex it adopts a single conformation which interacts with the AMG OE1 atom through a water molecule. The loop around Arg329 undergoes a small movement (Fig. 2*b*) in the complex (about 0.5 Å), with the main change in the complex being in the side chain of Arg329, which moves 2 Å closer to OE2 of AMG but is still unable to form a proper contact (distance of ∼4.7 Å). Like-

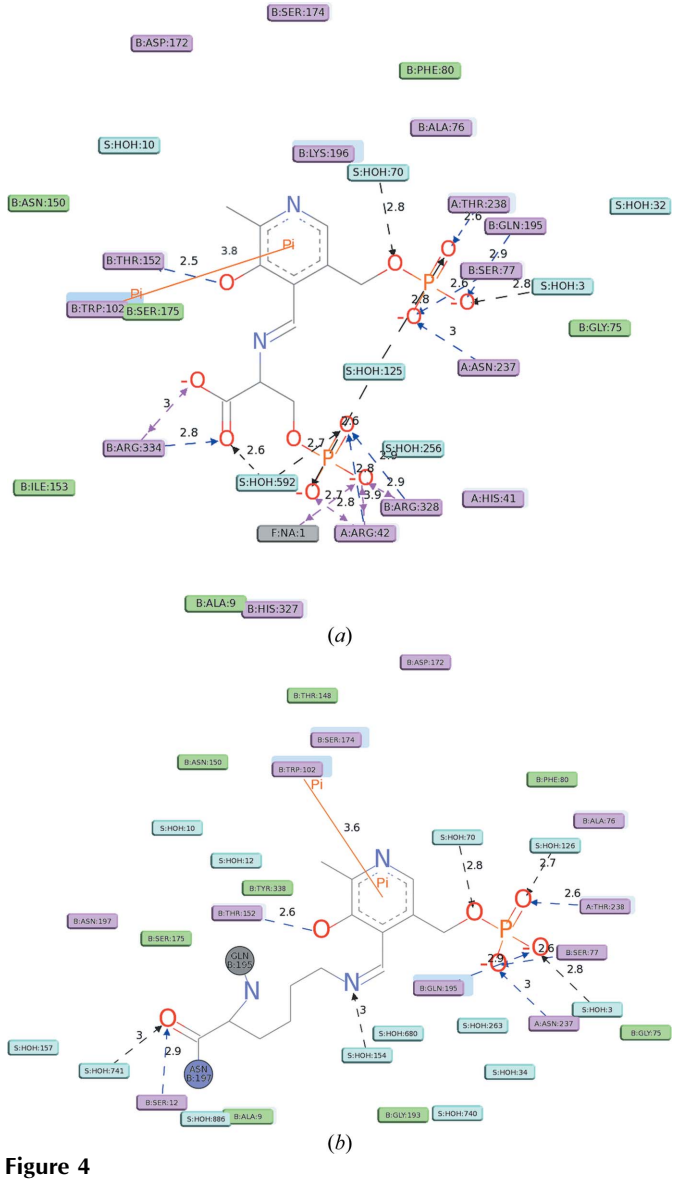

Figure 4
Two-dimensional diagram of the interactions between active-site residues and (*a*) PLP–PSER and (*b*) PLP. The colouring of the interactions is as follows: charge interaction, magenta dashed line with arrows at both ends; hydrogen bonds to side chain, blue dashed line with arrow at hydrogen-bond acceptor; hydrogen bond to main chain, green dashed line with arrow at hydrogen-bond acceptor; hydrogen bond to non-amino acid, black dashed line with arrow at hydrogen-bond acceptor; magenta-coloured residues, hydrogen bonds, polar and charge interactions; green-coloured residues, van der Waals interactions. Blue shading around residues or ligand atoms indicates solvent accessibility. This figure was created with *Discovery Studio* (http://www.accelrys.com).

wise, the loop around Arg42 does not change position significantly and only the side chain of Arg42 is adjusted to optimize contact with the OE1 atom of AMG (2.7 Å from Arg42 NH2).

4. Discussion

The structure of *Ba*PSAT in the presence of PSER was determined at 1.5 Å resolution and was compared with the structure of the unligated enzyme at 1.6 Å resolution. The two structures belonged to the same space group and the crystals used were grown under the same crystallization conditions. In addition, structural comparison was carried out with the free structure of *Ba*PSAT in space group $P2_12_12$ previously determined at 1.68 Å resolution using different crystallization conditions. These comparisons allowed a more detailed understanding of the conformational changes that occur in the enzyme–substrate complex and helped in excluding the influence of crystal packing from the observed changes. However, the extent of the conformational changes varies in the two crystal forms, possibly owing to the different flexibilities of the loops, as indicated by the locally elevated temperature factors in the free *Ba*PSAT structures.

*Ba*PSAT–PSER crystallizes as a dimer with a PSER attached to each PLP. In the free *Ba*PSAT structure PLP forms a Schiff-base linkage to Lys196, as expected. In the complex the link is broken and PLP is found in the form of an external aldimine that corresponds to an intermediate in the catalytic reaction. The binding of PSER is assisted by the formation of a phosphate-binding site consisting of His327 and Arg328 from one subunit and His41 and Arg42 from the second subunit in the functional PSAT dimer. In addition, a third Arg residue, Arg334, stabilizes the amino acid through interactions with the α-carboxylate group of PSER.

Several interactions that are present in the complex are also found in the free structure. For instance, Trp102 is aligned parallel to the PLP ring in both structures. Its contribution to the catalytic activity has recently been demonstrated by mutagenesis studies using a PSAT from the enteric human parasite *Entamoeba histolytica* (Mishra *et al.*, 2012). It was proposed that the indole ring is important for the stacking interactions. In the *Ba*PSAT–PSER complex Trp102 could offer further stabilization through a hydrogen bond to the α-carboxylate OXT atom. Thus, the indole ring of Trp102 may also play a role in correct positioning of the substrate.

Conformational changes in the structures of aspartate aminotransferase (AAT) in complex with various substrates or substrate analogues have been reported previously (Hammes, 2002). Domain movement has been observed in mitochondrial AAT (McPhalen *et al.*, 1992). It has been established that the small domain moves towards the large domain and that residues at

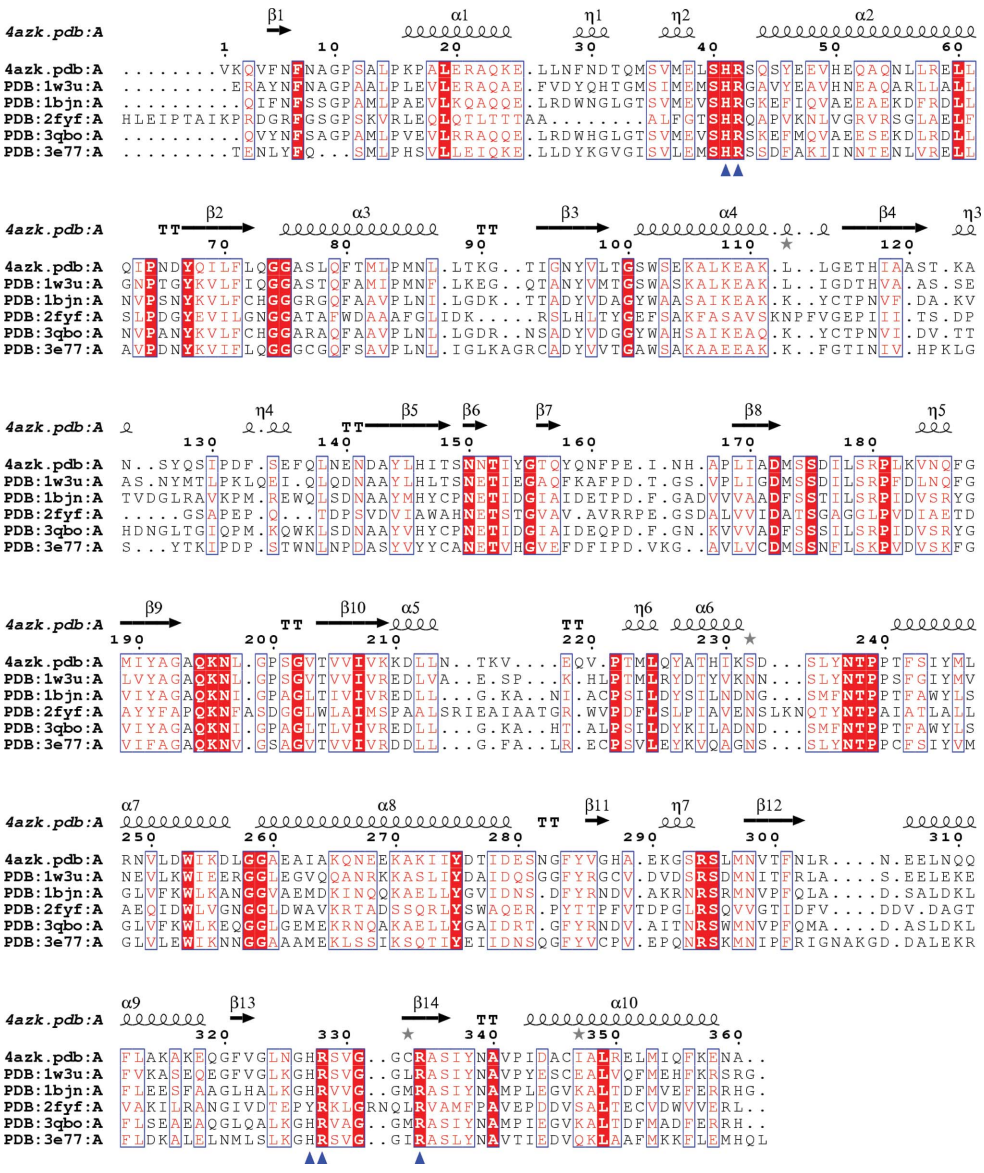

Figure 5
Structure-based sequence alignment of PSAT from various sources. The interacting residues are indicated by blue arrows. 1w3u, *B. circulans* var. *alkalophilus* PSAT (Kapetaniou *et al.*, 2006); 1bjn, *Ec*PSAT; 2fyf, *M. tuberculosis* PSAT (*MtB*PSAT; Coulibaly *et al.*, 2012); 3qbo, *Y. pestis* CO92 PSAT (Center for Structural Genomics of Infectious Diseases, unpublished work); 3e77, human PSAT (Structural Genomics Consortium, unpublished work). The figure was created with *ESPript* (Gouet *et al.*, 1999).

the entrance to the active site are reorganized to form a lid over the active site (Hayashi *et al.*, 2003). Various conformational changes in aminotransferases have been associated with dual substrate recognition for effective binding of diverse substrates (Hirotsu *et al.*, 2005). Structural analysis of *Ba*PSAT–PSER shows that the positions of the two domains and those of the subunits remain unchanged. The observed conformational changes are local and are unable to induce large movements in the structure. PSAT therefore appears to employ a local reorganization of the active site as a means of substrate recognition.

Structural comparison with the *Ec*PSAT–AMG complex revealed striking differences between the two complexes. However, it must be noted that the *Ec*PSAT–AMG complex has AMG bound in only one subunit as a result of crystallographic steric constraints in the second subunit. Moreover, the calculated electron density for the bound AMG indicates a low occupancy for the substrate analogue. It is possible that the presence of the methyl group in AMG could have created some steric hindrance that affects the correct positioning of the substrate analogue in the active site. These observations may explain the differences between the two complexes, particularly the lack of loop movements in *Ec*PSAT–AMG. On the other hand, the enzyme may exhibit a different response to each substrate in accordance with the dual substrate-recognition mechanism.

Four residues participate in recognition of the substrate phosphate group by creating a positively charged clamp around the phosphate anion. It has previously been reported (Basurko *et al.*, 1999) that the K_m values for PSER and L-glutamate of the human enzyme differ considerably (35 μM and 1.2 mM, respectively). In the case of L-glutamate as a substrate, the γ-carboxylate group and *Ec*PSAT Arg329 are far away and do not interact, at least directly, despite the conformational change that places the side chain of Arg329 closer to the γ-carboxylate group in the complex. This difference may also explain the ability of the active site to recognize different substrates characterized by the same or different lengths through alterations in the position of the Arg residue. Notably, PSAT from *B. circulans* var. *alkalophilus* has been reported to be responsible for most of the AAT activity in this bacterium (Battchikova *et al.*, 1996). In addition, *Ec*PSAT has also been found to be able to accept aspartate as a substrate (Hester *et al.*, 1999). As aspartate has a reduced side-chain length compared with glutamate, its recognition by PSAT could be explained by the flexibility of the Arg328 residue and the conformational changes described above. The importance of Arg328, especially in phosphate recognition, is further supported by the structure of a putative serine aminotransferase from *Pyrococcus horikoshii* OT3 (PDB entry 2dr1; RIKEN Structural Genomics/Proteomics Initiative, unpublished work), which has a glycine residue structurally aligned with Arg328 of *Ba*PSAT.

Cofactor rotation has been observed in *Salmonella typhimurium O*-acetylserine sulfhydrylase during formation of the external aldimine (Burkhard *et al.*, 1999). In the *Ec*PSAT–AMG structure the cofactor was found to be rotated by approximately 30° compared with that in the free enzyme. In contrast, a subtle (approximately 5°) rotation in the position of the cofactor was found in the *Ba*PSAT–PSER complex. However, no clear conclusion can be drawn here on the position of the ring owing to potential X-ray-induced conformational changes during data collection from PLP-containing enzymes (Dubnovitsky, Ravelli *et al.*, 2005).

Human PSAT has been implicated in cancer and has recently emerged as a target for drug intervention. The structure of human PSAT has been determined to 2.5 Å resolution (PDB entry 3e77; Structural Genomics Consortium, unpublished work) and shows 45.6% sequence identity to *Ba*PSAT over 346 aligned residues. The active site exhibits similarities to that of *Ba*PSAT, including the flexible Arg45 (structurally equivalent to Arg42 of *Ba*PSAT) and Arg336 (structurally equivalent to Arg328 of *Ba*PSAT). However, the side chains of Arg45 and Arg336 have not been modelled in human PSAT owing to their high flexibility. The two structures of *Ba*PSAT presented here could therefore act as models to predict the binding mode and potential interactions of various chemical compounds in the active site of human PSAT. Moreover, the recently determined crystal structure of PSAT from *Mycobacterium tuberculosis* (Coulibaly *et al.*, 2012) opens further opportunities for use of the described binding studies in the design of selective inhibitors, preferably with a phosphate group to take advantage of the phosphate-binding site. However, it must be pointed out that *M. tuberculosis* PSAT (*MtB*PSAT) has a Tyr at the position of His327 of *Ba*PSAT, a replacement that might affect the substrate-binding mechanism. The structure shows a bound sulfate ion that coincides with the phosphate group of L-phosphoserine. However, Arg342 (which is structurally equivalent to Arg328 of *Ba*PSAT) is characterized by some disorder, as shown by the quality of the electron-density map and the higher temperature factor (17.6 and 20.8 Å^2 in subunits *A* and *B*, respectively) compared with the rest of the structure (∼10.8 Å^2 for both subunits). The guanidium group of Arg342 is close to the sulfate ion, but points outwards in a considerably different position from that of Arg328 of *Ba*PSAT–PSER (Supplementary Fig. S2). These observations suggest that the

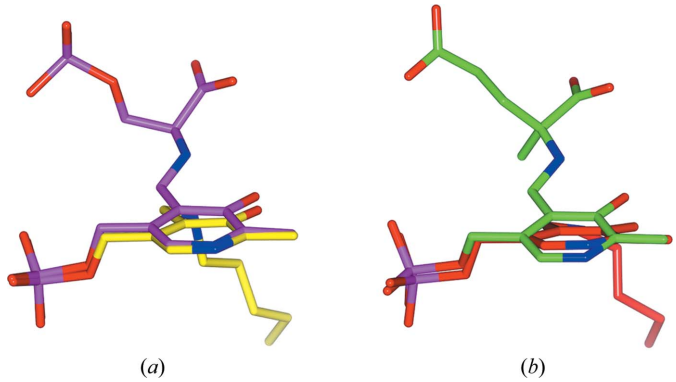

Figure 6
Close-up view of the PLP position in the active site. (*a*) *Ba*PSAT–PSER (yellow, PLP; magenta, PLP–PSER). (*b*) *Ec*PSAT–AMG (red, PLP; green, PLP–AMG).

binding of a sulfate ion is unable to promote stabilization effects similar to those observed with L-phosphoserine. In support of this, the average temperature factors (15.0 Å^2 in subunit *A* and 17.0 Å^2 in subunit *B*) for residues 341–346 are higher than the average temperature factors for the entire protein. A crystal structure of *MtB*PSAT with bound substrate would certainly provide further insights into the substrate-binding mechanism of *MtB*PSAT and allow a detailed direct comparison with *Ba*PSAT.

5. Conclusions

The crystal structure of *Ba*PSAT–PSER demonstrates that *Ba*PSAT lacks domain and subunit movements during substrate binding. The observed conformational changes are mostly local and result in the formation of a tight binding site for the phosphate group of PSER. In comparison with the previous determined structure of *Ec*PSAT–AMG, the *Ba*PSAT–PSER structure suggests a mechanism for distinguishing between the phosphate and the carboxylate group of the bound substrates. The results presented here will help in better understanding the catalytic mechanism of PSAT and could provide guidelines for the design of small molecules as potential inhibitors of human and microbial PSATs.

We thank the staff of the EMBL PX beamline X13 at the DORIS storage ring (DESY, Hamburg) and of the MAX-lab PX beamline I711 (Lund) for help during data collection. We are grateful to N. Battchikova, M. Koivulehto and T. Korpela, University of Turku for generously providing the BALC PSAT plasmid. This work was financially supported by the Academy of Finland (grant Nos. 121278 and 78699). The infrastructure support provided by Biocenter Finland is greatly acknowledged.

References

Adams, P. D. *et al.* (2010). *Acta Cryst.* D**66**, 213–221.
Baek, J. Y., Jun, D. Y., Taub, D. & Kim, Y. H. (2003). *Biochem. J.* **373**, 191–200.
Basurko, M. J., Marche, M., Darriet, M. & Cassaigne, A. (1999). *IUBMB Life*, **48**, 525–529.
Battchikova, N., Himanen, J.-P., Ahjolahti, M. & Korpela, T. (1996). *Biochim. Biophys. Acta*, **1295**, 187–194.
Burkhard, P., Tai, C.-H., Ristroph, C. M., Cook, P. F. & Jansonius, J. N. (1999). *J. Mol. Biol.* **291**, 941–953.
Chen, V. B., Arendall, W. B., Headd, J. J., Keedy, D. A., Immormino, R. M., Kapral, G. J., Murray, L. W., Richardson, J. S. & Richardson, D. C. (2010). *Acta Cryst.* D**66**, 12–21.
Coulibaly, F., Lassalle, E., Baker, H. M. & Baker, E. N. (2012). *Acta Cryst.* D**68**, 553–563.
Cruickshank, D. W. J. (1999). *Acta Cryst.* D**55**, 583–601.
Dubnovitsky, A. P., Kapetaniou, E. G. & Papageorgiou, A. C. (2003). *Acta Cryst.* D**59**, 2319–2321.
Dubnovitsky, A. P., Kapetaniou, E. G. & Papageorgiou, A. C. (2005). *Protein Sci.* **14**, 97–110.
Dubnovitsky, A. P., Ravelli, R. B. G., Popov, A. N. & Papageorgiou, A. C. (2005). *Protein Sci.* **14**, 1498–1507.
Emsley, P. & Cowtan, K. (2004). *Acta Cryst.* D**60**, 2126–2132.
Gouet, P., Courcelle, E., Stuart, D. I. & Métoz, F. (1999). *Bioinformatics*, **15**, 305–308.
Hammes, G. G. (2002). *Biochemistry*, **41**, 8221–8228.
Hayashi, H., Mizuguchi, H., Miyahara, I., Nakajima, Y., Hirotsu, K. & Kagamiyama, H. (2003). *J. Biol. Chem.* **278**, 9481–9488.
Hester, G., Stark, W., Moser, M., Kallen, J., Marković-Housley, Z. & Jansonius, J. N. (1999). *J. Mol. Biol.* **286**, 829–850.
Hirotsu, K., Goto, M., Okamoto, A. & Miyahara, I. (2005). *Chem. Rec.* **5**, 160–172.
Kabsch, W. & Sander, C. (1983). *Biopolymers*, **22**, 2577–2637.
Kapetaniou, E. G., Thanassoulas, A., Dubnovitsky, A. P., Nounesis, G. & Papageorgiou, A. C. (2006). *Proteins*, **63**, 742–753.
Koning, T. J. de, Snell, K., Duran, M., Berger, R., Poll-The, B.-T. & Surtees, R. (2003). *Biochem. J.* **371**, 653–661.
Krissinel, E. & Henrick, K. (2004). *Acta Cryst.* D**60**, 2256–2268.
McCoy, A. J., Grosse-Kunstleve, R. W., Adams, P. D., Winn, M. D., Storoni, L. C. & Read, R. J. (2007). *J. Appl. Cryst.* **40**, 658–674.
McNicholas, S., Potterton, E., Wilson, K. S. & Noble, M. E. M. (2011). *Acta Cryst.* D**67**, 386–394.
McPhalen, C. A., Vincent, M. G., Picot, D., Jansonius, J. N., Lesk, A. M. & Chothia, C. (1992). *J. Mol. Biol.* **227**, 197–213.
Mishra, V., Kumar, A., Ali, V., Nozaki, T., Zhang, K. Y. J. & Bhakuni, V. (2012). *Amino Acids*, **43**, 483–491.
Moriarty, N. W., Grosse-Kunstleve, R. W. & Adams, P. D. (2009). *Acta Cryst.* D**65**, 1074–1080.
Ojala, P., Sundström, J., Grönroos, J. M., Virtanen, E., Talvinen, K. & Nevalainen, T. J. (2002). *Electrophoresis*, **23**, 1667–1676.
Otwinowski, Z. & Minor, W. (1997). *Methods Enzymol.* **276**, 307–326.
Pollari, S., Käkönen, S. M., Edgren, H., Wolf, M., Kohonen, P., Sara, H., Guise, T., Nees, M. & Kallioniemi, O. (2011). *Breast Cancer Res. Treat.* **125**, 421–430.
Urzhumtseva, L., Afonine, P. V., Adams, P. D. & Urzhumtsev, A. (2009). *Acta Cryst.* D**65**, 297–300.
Vié, N., Copois, V., Bascoul-Mollevi, C., Denis, V., Bec, N., Robert, B., Fraslon, C., Conseiller, E., Molina, F., Larroque, C., Martineau, P., Del Rio, M. & Gongora, C. (2008). *Mol. Cancer*, **7**, 14.